Terahertz phase slips in striped $La_{2-x}Ba_xCuO_4$

D. Fu[1], D. Nicoletti[1], M. Fechner[1], M. Buzzi[1], G. D. Gu[2], A. Cavalleri[1,3]*

[1] *Max Planck Institute for the Structure and Dynamics of Matter, 22761 Hamburg, Germany*

[2] *Condensed Matter Physics and Materials Science Department, Brookhaven National Laboratory, Upton, NY, United States*

[3] *Department of Physics, Clarendon Laboratory, University of Oxford, Oxford OX1 3PU, United Kingdom*

* e-mail: andrea.cavalleri@mpsd.mpg.de

Supplemental Material

S1. Simulation of the Josephson phase dynamics with the sine-Gordon equation

To simulate the dynamics of the Josephson junction we solved the one-dimensional sine-Gordon equation using a finite difference approach. Hereby, we assumed a single Josephson junction with semi-infinite layers, having the extended dimension along the x direction. The evolution of the Josephson phase, $\varphi(x,t)$, is described by

$$\frac{\partial^2 \varphi(x,t)}{\partial t^2} + 2\gamma \frac{\partial \varphi(x,t)}{\partial t} + \omega_{JPR}^2 \sin\varphi(x,t) = \frac{c^2}{\varepsilon} \frac{\partial^2 \varphi(x,t)}{\partial x^2}. \tag{S1}$$

Here, ω_{JPR} is the plasma frequency, c the speed of light, ε the relative dielectric permittivity, and γ a damping factor accounting for the quasiparticle tunneling current. We used tabulated values for ω_{JPR} and ε, and set γ as a fitting parameter.

We incorporated the THz driving field, $E(t)$, by setting the spatial and temporal phase evolution at the interface to the following condition:

$$\left.\frac{\partial \varphi(x,t)}{\partial t}\right|_{x=0} - c \left.\frac{\partial \varphi(x,t)}{\partial x}\right|_{x=0} = 2\omega_{JPR} \frac{E(t)}{E_c} \quad , \tag{S2}$$

with $E_c = \Phi_0 \omega_{JPR}/(2\pi d)$, where Φ_0 is the flux quantum and d the distance between adjacent superconducting layers. Note that this is the same approach as that used in our previous works (see *e.g.*, Ref. [i]). For the simulations shown in Fig. 1 of the main text, we used the following values: $\omega_{JPR} = 0.53$ THz, $\varepsilon = 25$, $\gamma = 0.37$ THz, and $d = 10$ Å. The temporal and spatial grid have been tested for stability and convergence and finally set to $\Delta x = 1$ μm and $\Delta t = 4$ fs.

S2. Experimental methods

Large single crystals of $La_{2-x}Ba_xCuO_4$ with $x = 0.095$ and $x = 0.115$ (~4 mm diameter), grown by transient solvent method, were studied here. These crystals belonged to the same batch of samples as reported in earlier works[i,ii,iii], and were cut and polished along the ac surface.

Laser pulses with 800-nm wavelength, ~100-fs duration and ~3.5 mJ energy were split into 2 parts (99% - 1%) with a beam splitter. The most intense beam was used to generate terahertz (THz) pulses by optical rectification in $LiNbO_3$ with the tilted pulse front technique[iv]. These pump pulses were collimated and focused at normal incidence onto the sample, and they were *s*-polarized (*i.e.*, perpendicular to the plane of incidence), corresponding to the crystallographic direction perpendicular to the CuO_2 planes (parallel to the c axis).

The THz beam spot diameter at the sample position was ~1.5 mm, with a maximum attainable field strength of ~165 kV/cm. The incident field strength was adjusted using a pair of wire grid polarizers. The peak electric field value at the sample position was estimated either by using a calibrated pyroelectric detector and accurately measuring the spot size, or by placing a GaP crystal in place of the sample itself and electro-optically sampling with a weak near-infrared gate beam. Both methods provided values in agreement within 20%.

An example time trace of the pump THz field, as well as the corresponding spectrum, are shown in Fig. S1. The spectrum is superimposed on the loss function of both samples measured in the superconducting state at the lowest temperature[i,v,vi]. This quantity shows a peak at the Josephson plasma frequency, providing a clear indication of the resonant pump condition, particularly for LBCO 9.5%.

The Electric Field Induced Second Harmonic (EFISH)[vii] was generated from 800-nm wavelength probe pulses (1% of the laser output). These were shone onto the sample with polarization along the c axis and scanned in time through the profile of the THz pump. In equilibrium and without pump, no second harmonic was found. The pump-induced 400-nm second harmonic intensity, $I_{SHG}(t)$, generated at the surface was detected with a photomultiplier. By scanning the time delay, t, between THz pump and NIR probe, the full second harmonic temporal profile could be determined.

In order to eliminate the effect of any slow drift in the signal, which could have originated for example from the accumulation of ice on the sample surface, we have undertaken a measurement procedure which involved the acquisition of scans at a given temperature interspersed with reference scans at a temperature higher than all relevant temperatures in the given compound. These reference scans were acquired at $T_{ref} = 50\,\text{K} > T_C, T_{SO}, T_{CO}$ for LBCO 9.5% and at $T_{ref} = 70\,\text{K} > T_C, T_{SO}, T_{CO}$ for LBCO 11.5%, after verifying in both materials that the EFISH signal was independent of temperature for all $T > T_{ref}$. Each measurement at these temperature pairs was then repeated several times, and the data were statistically analyzed to estimate the error bars shown, for example, in Fig. 2(a) of the main text.

An example of data processing on a single set of measurements is reported in Fig. S2. Therein, we show how time traces acquired at a certain $T < T_{ref}$ and at $T = T_{ref}$ are first subtracted in time domain and then Fourier transformed. Virtually identical results were obtained by performing the subtraction in frequency domain.
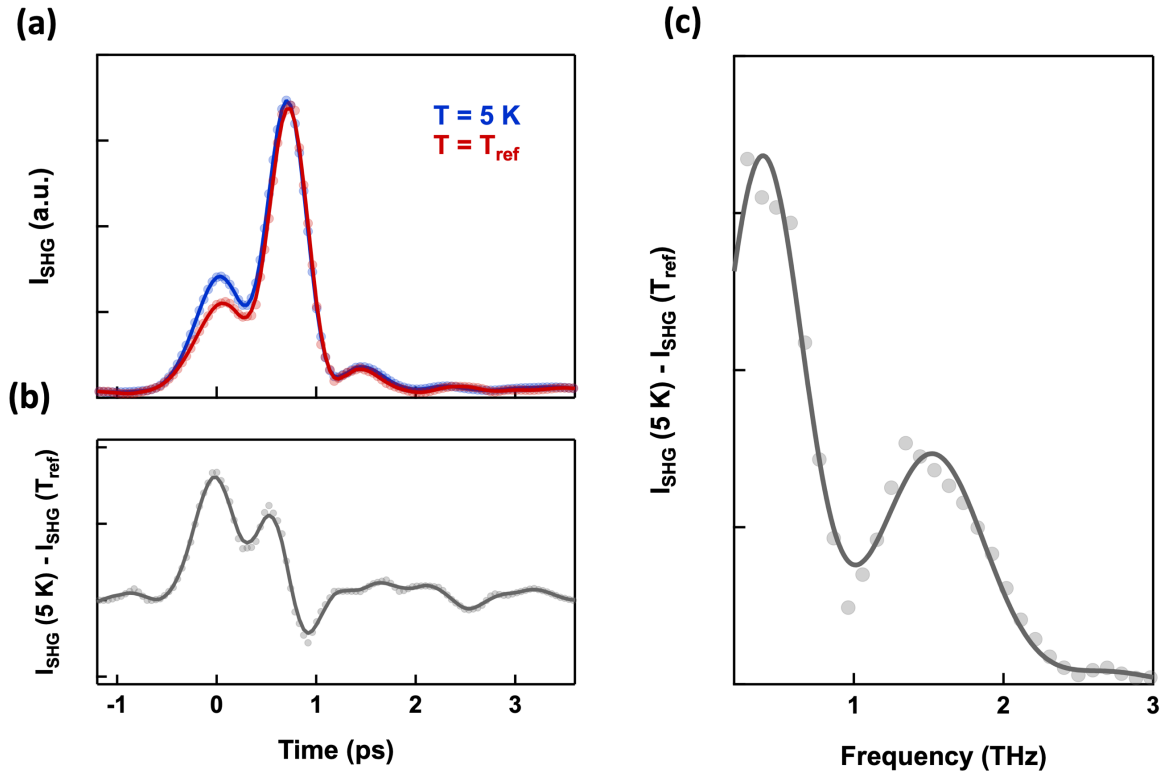
S3. Additional data sets

In this section we report additional data sets to complement those shown in the main text. In particular, these are the original spectra from which we extracted, via multi-Gaussian fits, the dependence of I_ω and $I_{3\omega}$ on the peak driving THz field for LBCO 11.5% at $T = 5$ K (Fig. 2(b) and Fig. 2(c)) and $T = 30$ K (Fig. 3(c) and Fig. 3(d)), as well as the temperature dependences of the same quantities for both compounds (Fig. 3(a) and Fig. 3(b)).

In Fig. S3 we report THz field dependent spectra acquired in LBCO 11.5% at two temperatures ($T < T_C$ and $T_C < T < T_{CO}$), displaying a behavior virtually identical to that measured in the superconducting phase of LBCO 9.5% (Fig. 2(a) of the main text). Fig. S4 shows instead the variation of the second harmonic spectra as a function of temperature in both compounds, all acquired at the same peak THz field value of $\sim$165 kV/cm. As discussed for Fig. 3(a) and Fig. 3(b) of the main text, while in LBCO 9.5% the response disappears at $T_C = 32$ K, in LBCO 11.5% it extends all the way to T_{CO}.
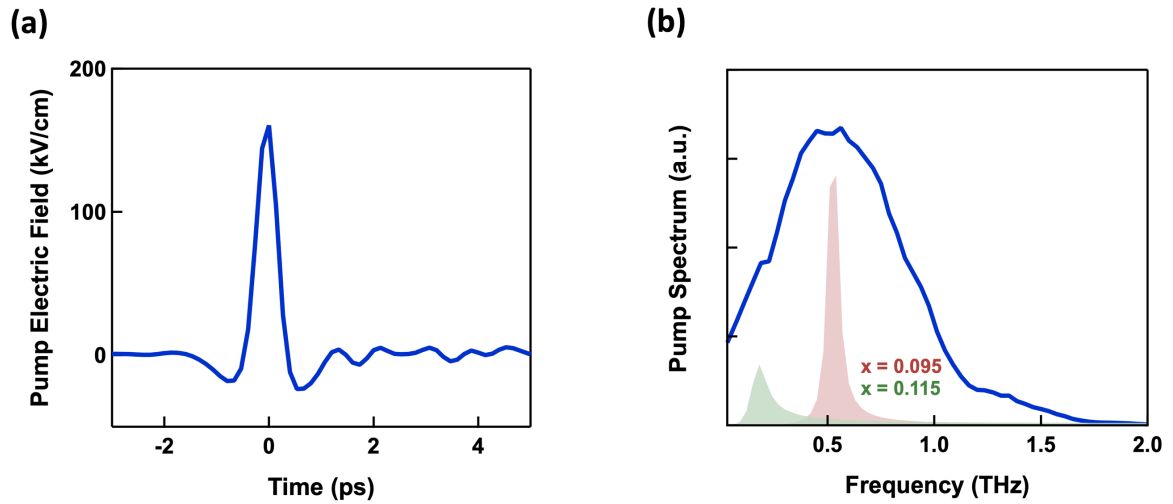
Figure S1. (a) Electric field profile of the THz pump pulses, measured at the sample position via electro-optic sampling in a 300-µm thick GaP crystal. (b) Blue curve: Corresponding Fourier transform spectrum of the time trace in (a). The red and green shadings indicate the energy loss function of $La_{1.905}Ba_{0.095}CuO_4$ and $La_{1.885}Ba_{0.115}CuO_4$, respectively, measured in the equilibrium superconducting state at $T = 5\,\text{K} < T_C$. Notably, the Josephson plasmon of both compounds (peak frequency in the loss function) can be driven at (or close to) resonance by the THz pump field.

(a)

I_{SHG} (a.u.)

T = 5 K
T = T_{ref}

(b)

I_{SHG} (5 K) - I_{SHG} (T_{ref})

(c)

I_{SHG} (5 K) - I_{SHG} (T_{ref})

Time (ps)

Frequency (THz)

Figure S2. (a) Time-dependent Electric Field Induced Second Harmonic (EFISH) signal measured in $La_{1.905}Ba_{0.095}CuO_4$ at $T = 5$ K $< T_C$ (blue) and at the reference temperature $T_{ref} = 50$ K for a THz peak electric field of ~165 kV/cm. **(b)** Normalized EFISH signal, obtained by subtracting the two curves in (a) in time domain. **(c)** Frequency-dependent normalized EFISH response, obtained by Fourier transforming the curve in (b). This quantity is the same as that shown in Fig. 2(a) of the main text, as well as in Fig. S3 and Fig. S4 of the Supplemental Material.
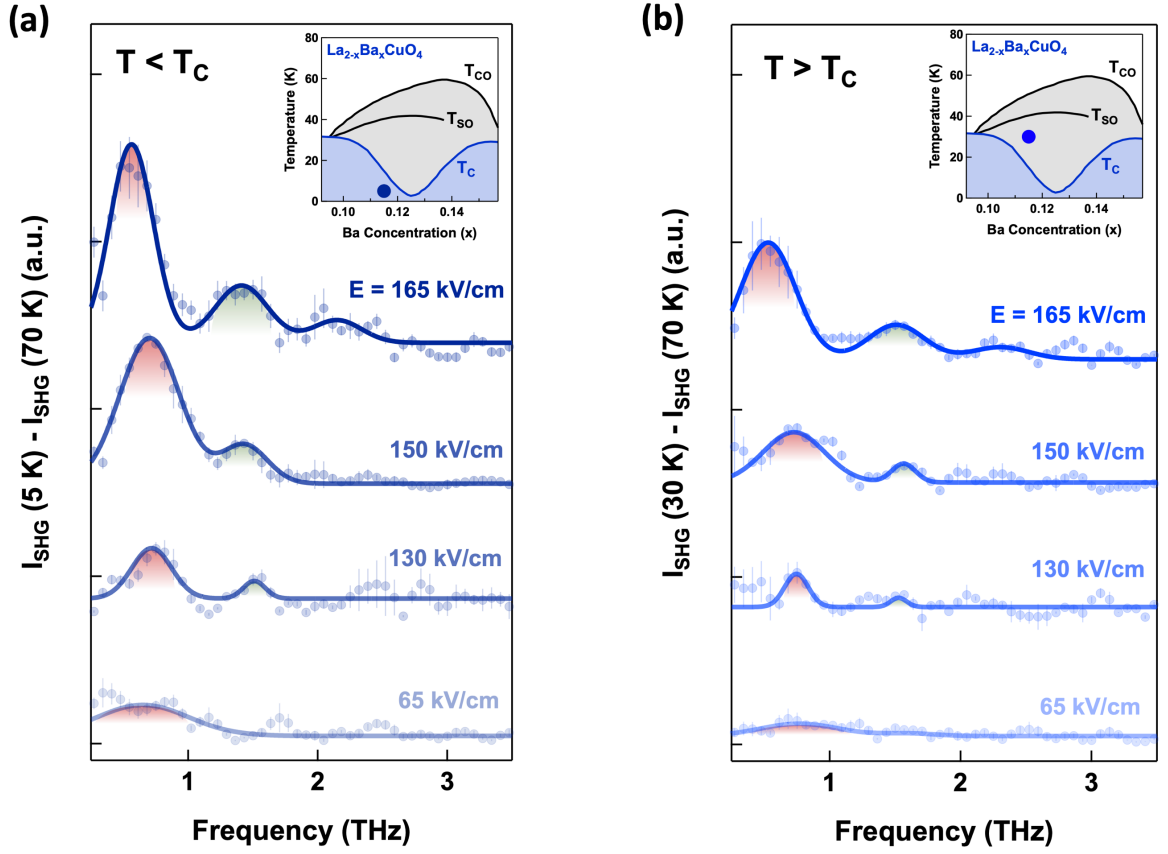
Figure S3. (a) Fourier transform of the second harmonic intensity measured in superconducting $La_{1.885}Ba_{0.115}CuO_4$ at $T = 5$ K $< T_C$ for different THz peak driving fields, after subtraction of the same quantity measured at $T > T_C, T_{SO}, T_{CO}$. The spectra have been vertically offsetted maintaining their relative amplitude. Uncertainty bars are standard errors estimated from different measurement sets. The peaks at $\sim\omega_{drive}$ and $\sim 3\omega_{drive}$ are shaded in red and green, respectively. Inset: Temperature-doping phase diagram of $La_{2-x}Ba_xCuO_4$, where the exact location of the investigated material is indicated by a blue circle. Here, T_{CO}, T_{SO}, and T_C are the charge-order, spin-order, and superconducting transition temperature, respectively. **(b)** Same quantity as in (a), measured in $La_{1.885}Ba_{0.115}CuO_4$ at $T = 30$ K $> T_C$. Inset: Temperature-doping phase diagram as in (a).
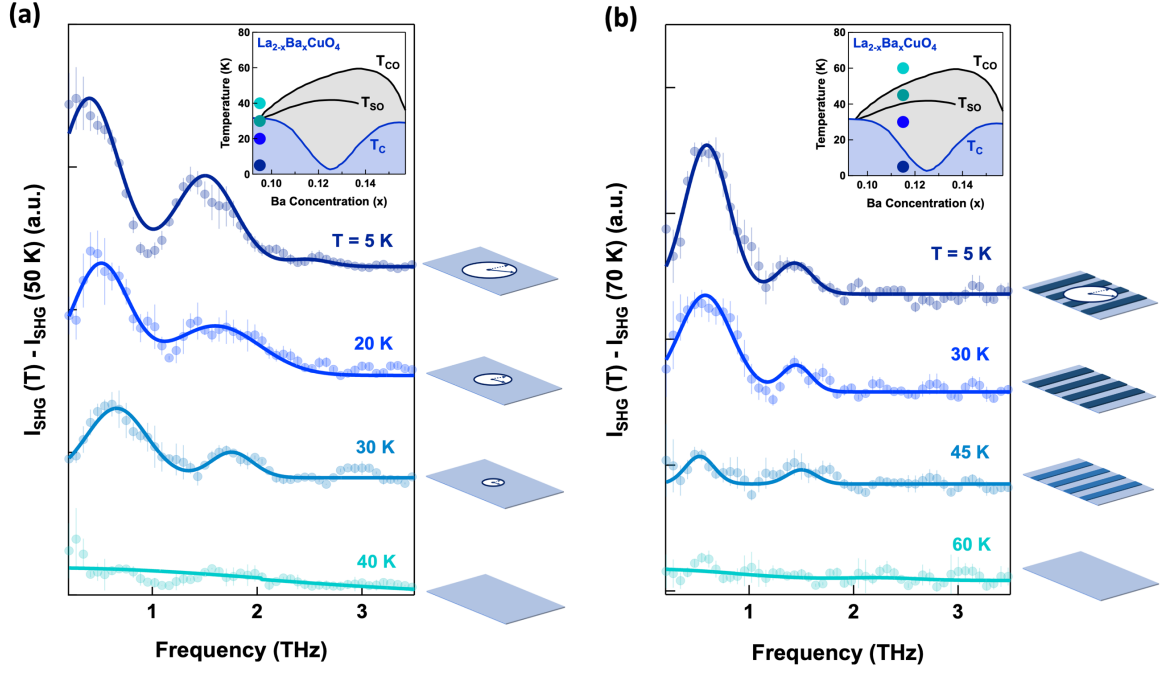
Figure S4. (a) Fourier transform of the second harmonic intensity measured in La$_{1.905}$Ba$_{0.095}$CuO$_4$ at different temperatures, for a peak THz field of ~165 kV/cm, after subtraction of the same quantity measured at $T = 50$ K $> T_C$. The spectra have been vertically offsetted maintaining their relative amplitude. Uncertainty bars are standard errors estimated from different measurement sets. Inset: Temperature-doping phase diagram of La$_{2-x}$Ba$_x$CuO$_4$, where the measured temperatures are indicated by circles (T_{CO}, T_{SO}, and T_C are the charge-order, spin-order, and superconducting transition temperature, respectively). The graphics on the right represent the progressive reduction of the amplitude of the superconducting order parameter (clock diameter) with increasing temperature and its disappearance above T_C. **(b)** Same quantity as in (a) measured in La$_{1.885}$Ba$_{0.115}$CuO$_4$ at different temperatures across T_C, T_{SO}, and T_{CO}, for a ~165 kV/cm driving field. Normalization is done here by $T = 70$ $K >$ T_C, T_{SO}, T_{CO}. Inset: Temperature-doping phase diagram as in (a). The graphics on the right represent the disappearance of the macroscopic superconducting order parameter (clock) when crossing T_C, as well as the gradual fainting of the stripe order, which coexists with superconductivity at $T < T_C$, and survives all the way up to $T = T_{CO}$.

REFERENCES

[i] S. Rajasekaran, E. Casandruc, Y. Laplace, D. Nicoletti, G. D. Gu, S. R. Clark, D. Jaksch, and A. Cavalleri, "Parametric amplification of a superconducting plasma wave", Nat. Phys. **12**, 1012-1017 (2016).

[ii] C. C. Homes, M. Hücker, Q. Li, Z. J. Xu, J. S. Wen, G. D. Gu, and J. M. Tranquada, "Determination of the optical properties of $La_{2-x}Ba_xCuO_4$ for several dopings, including the anomalous x=1/8 phase", Phys. Rev. B **85**, 134510 (2012).

[iii] S. Rajasekaran, J. Okamoto, L. Mathey, M. Fechner, V. Thampy, G. D. Gu, and A. Cavalleri, "Probing optically silent superfluid stripes in cuprates", Science **359**, 575–579 (2018).

[iv] J. Hebling, K.-L. Yeh, M.C. Hoffmann, B. Bartal, and K.A. Nelson, "Generation of high-power terahertz pulses by tilted-pulse-front excitation and their application possibilities", J. Opt. Soc. Am. B **25**, B6–B19 (2008).

[v] D. Nicoletti, E. Casandruc, Y. Laplace, V. Khanna, C. R. Hunt, S. Kaiser, S. S. Dhesi, G. D. Gu, J. P. Hill, A. Cavalleri, "Optically-induced superconductivity in striped $La_{2-x}Ba_xCuO_4$ by polarization-selective excitation in the near infrared", Phys. Rev. B **90**, 100503(R) (2014).

[vi] D. Nicoletti, D. Fu, O. Mehio, S. Moore, A. S. Disa, G. D. Gu, and A. Cavalleri, "Magnetic-Field Tuning of Light-Induced Superconductivity in Striped $La_{2-x}Ba_xCuO_4$", Phys. Rev. Lett. **121**, 267003 (2018).

[vii] M. Fiebig, V. V. Pavlov, and R. V. Pisarev, "Second-harmonic generation as a tool for studying electronic and magnetic structures of crystals: review", J. Opt. Soc. Am. B **22**, 96-118 (2005).